ANNALS OF GEOPHYSICS, 69, 2026; doi:10.4401/ag-9458
OPEN ACCESS

Hydrogeochemical Anomaly in the Aegean Region, Western Türkiye: Possible relation to Santorini Island (Greece) Earthquake Swarm

Nurettin Yakupoğlu[*,1]

[(1)] İstanbul Technical University, Faculty of Mines, Department of Geological Engineering, İstanbul, Türkiye

Article history: received October 16, 2025; accepted March 19, 2026

Abstract

Hydrogeochemical anomalies in groundwater systems are recognized as potential earthquake precursors, yet their detectability varies depending on long-term monitoring techniques as well as geological and structural features of observation sites. This study examines 28-month long spring water record comparing the seasonal variations, rainfall contribution and propose a possible link between precursory signals for February-March 2025 Santorini earthquake swarm which comprised approximately 2,700 events and a cumulative seismic energy release equivalent to Mw 6.1-6.2. Monitoring of the Naz-01 spring in Nazilli, Türkiye, displays optimal level of EC (90 µS/cm) and have an approximately 180 days long positive anomaly reaching up to (180 µS/cm) which revealed marked increases in electrical conductivity as well as major ion concentrations before the onset of seismic activity. However, two other spring waters (Boz-01 and Çine-01) has no distinct anomaly before or during the events. Moreover, while empirical precursor models would predict no detectable response at such distances for individual moderate events, the observed signal may be caused by the cumulative energy release from the swarm, which lies within the expected impact range for a single, larger equivalent source. The results suggest that structural connectivity between the source region and the monitoring site enabled efficient stress transfer and fluid-rock interaction, triggering measurable geochemical anomaly at Naz-01 spring. Conversely, seismic events of similar or greater magnitude occurring in structurally decoupled neighboring micro-plates (blocks) did not produce detectable anomalies at Boz-01 spring, contrarily Çine-01 as well. These observations emphasize that near fault located springs seems to be much more susceptible to the hydrogeochemical anomalies and tectonic connectivity is a way to show the reasoning why presence/absence of the anomalies in spring waters. These findings highlight the importance of monitoring the spring waters in a multi-disciplinary way to improve our understanding to the reliability of earthquake precursor detection with multiple monitoring sites and various monitoring techniques.

Keywords: Hydrogeochemical anomalies; Spring water; Earthquake precursors; Santorini; Aegean Sea

1. Introduction

The hydrogeochemical anomalies in groundwater systems are one of the tools to provide insights and better understanding on pre-earthquake researches (Rikitake, 1979, 1987; Dobrovolsky et al., 1979; Wakita, 1996). The relationship between crustal stress distribution and groundwater chemistry variations offers valuable insights for short-term earthquake forecasting, reflecting key crustal properties such as stress distribution, fluid-rock interaction, and fluid migration (Scholz et al., 1973; Nur, 1974; Doglioni et al., 2014; Martinelli and Dadomo, 2017; Martinelli and Tamburello, 2020; Martinelli et al., 2023). Geochemical precursor research is mainly based on soil and water-radon emanations that carefully analyzed positive anomalies occurring before the earthquakes (Thomas et al., 1986; Papastefanou et al., 1989; Abbad et al., 1995; Pulinets et al., 1997; İnan et al., 2008, 2010, 2012b, 2012c; Immè and Morelli, 2012; Ingebritsen and Manga, 2014; Woith, 2015; Seyis et al., 2022; Stoulos et al., 2024; Sahoo et al., 2025; Tverdyi et al., 2025) and hydrogeochemical research; including changes of water temperature andelemental distributions (Claesson et al., 2004) major/minor ion concentration (Tsunogai and Wakita, 1995; Toutain et al., 1997; Quattrocchi et al., 2000; Perez et al., 2008; Skelton et al., 2008, 2014, 2019; İnan et al., 2010, 2012a, 2012b, 2024; Barberio et al., 2017; Barbieri et al., 2021; Yan et al., 2024; Yakupoğlu et al., 2025), gas discharge rates (Sugisaki et al., 1996), stable isotopes (Skelton et al., 2014, 2019; Xiang and Peng, 2023; Zeng et al., 2025; Wang et al., 2025), pH level (Malakootian and Nouri, 2010; Barberio et al., 2017; Gori and Barberio, 2022; Luque-Espinar and Mateos, 2023), and electrical conductivity prior to earthquakes (Skelton et al., 2008; İnan et al., 2010, 2012a, 2012b, 2024; Luque-Espinar and Mateos, 2023; Yakupoğlu et al., 2025). However, such deep mixing processes are commonly associated with increased salinity and elevated concentrations of major ions, both of which are directly reflected in EC measurements related with or during seismic episodes, though the physical mechanisms, temporal characteristics, and spatial extent of such responses remain debated (Ingebritsen and Manga, 2014; Xiang and Peng, 2023; Martinelli et al., 2023). Among these parameters, electrical conductivity (EC) is a particularly sensitive proxy, as it integrates the combined effects of ionic strength, fluid provenance, and water-rock interaction. Variations in EC may reflect changes in salinity due to deep fluid contributions or shifts in groundwater mixing regimes driven by structural or hydrological reorganization. However, EC is also influenced by non-tectonic factors such as seasonal recharge, precipitation variability, and long-term hydrogeological evolution, requiring careful contextual interpretation. In this context, distinguishing between tectonically induced signals and local or environmental controls remains a central challenge in interpreting hydrogeochemical anomalies.

The Santorini Island in the South Aegean Sea (Fig. 1) is located in a significant geodynamic setting, including major volcanic eruptions (Friedrich, 2000) and earthquakes (Galanopoulos et al., 2005). In February-March 2025, the Santorini region experienced a significant earthquake swarm comprising 879 events with magnitudes exceeding Mw 3.0. When smaller-magnitude earthquakes are also considered (~2700 events), the cumulative seismic energy release is estimated at approximately 1×10^{14} joules (Toker et al., 2025); approximately equivalent of a 6.1-6.2 Mw event (Triantafyllou et al., 2025). Although this equivalence refers solely to the integrated energy release and does not imply dynamic or mechanical similarity, many studies conducted after these events, have focused mostly on the characteristics of the seismic events (Briole et al., 2025; Isken et al., 2025; Hufstetler et al., 2025; Mavroulis et al., 2025).

This study focusses on search of the possible pre-earthquake hydrogeochemical anomalies may be related to the February-March 2025 Santorini earthquake swarm by using three distinct spring waters and their changes in electrical conductivities and ion contents. A 28-month monitoring record reveals statistically elevated values relative to the long-term baseline, prompting examination of possible links between these variations and regional tectonic processes. This is the same spring water previously documented as susceptible to such precursory anomalies (Yakupoğlu et al., 2025) at Kuşadası 5.0 Mw earthquake (27 Jan 2024). Therefore, aim of this study is to find an probable evaluation on the potential link between the Santorini 2025 earthquake swarm and provide a cross correlation between observed pre-seismic hydrogeochemical anomalies and rainfall, seasonal variations and empirical precursor models (Dobrovolsky et al., 1979; Bowman et al., 1998; Martinelli and Tamburello, 2020), to provide a better understanding how a distant (~300 km) yet structurally connected groundwater systems can exhibit detectable responses prior to clustered seismic energy release. By doing so, main objective is not to establish a direct causal relationship, but to evaluate whether the observed anomalies are consistent with existing empirical precursor models and regional geological connectivity, while considered of the alternative hydrological and environmental explanations.

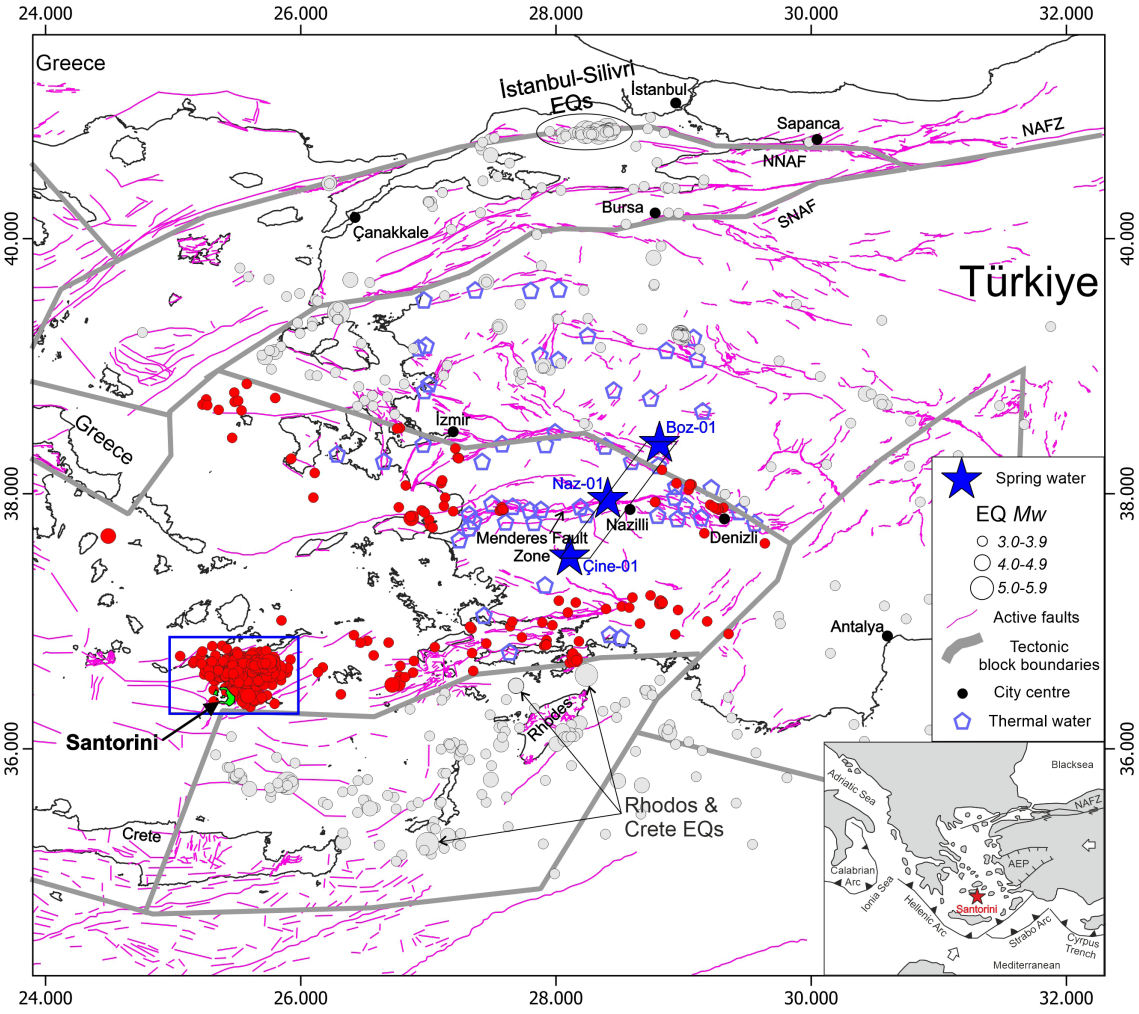

Figure 1. Location of the study area and tectonic setting. Map is constructed with longitude coordinate system, elevations are on wgs84 format. The inset map shows current tectonic setting of Aegean Sea and surroundings. Studied are Aegean Extensional Province (AEP) is indicated. Main map displays the active fault map of the Western Anatolia, Aegean Sea. Location of the spring waters (Naz-01, Çine-01 and Boz-01) are indicated as blue star. Black rectangle is the area of cross-section shown in Fig. 6. Magenta lines represent the active faults (Emre et al., 2012; Ganas et al., 2013). Plotted EQs cover the time between May 2023 to July 2025. Dark gray thick lines show the previously published microplate boundaries that is edited from Nyst and Thatcher (2004) and Reilinger et al. (2006). Santorini island is highlighted in green color. Light blue pentagons represent the thermal water sites around the region. MFZ: Menderes Fault Zone, NAFZ: North Anatolian Fault Zone, NNAF: Northern branch of North Anatolian Fault, SNAF: Southern branch of North Anatolian Fault Zone. All earthquakes (≥3) are plotted in red color (in-block EQs) and in gray color (out-block EQs) circles; diameters are scaled to earthquake magnitude (http://www.koeri.boun.edu.tr/sismo/zeqdb/).

2. Geological Setting

The Aegean Extensional Province (AEP) is among the most seismically active and rapidly deforming regions in Eurasia. N-S extension is primarily driven by the southwestward (~30 mm/yr) motion of southwestern Anatolia and southern Greece, combined with the Hellenic subduction system and distributed strike-slip faulting in the North Aegean Sea (Taymaz et al., 1991; Jackson, 1994; Bozkurt, 2003; Bozkurt and Mittwede, 2005; Jolivet et al., 2013) (Fig. 1). Major fault system is the Pliny-Strabo Fault Zone, accommodate significant portions of the Eurasia-South Aegean relative motion, leading to crustal thinning, high deformation rates, and elevated seismicity (Fig. 1).

Within this extensional setting, one of the most prominent geomorphological features of the Aegean Sea is the South Aegean Active Volcanic Arc which is formed as a result of the subduction of the African plate beneath the Aegean

microplate (Fig. 1). This arc hosts several Quaternary volcanic regions among which Christiana-Santorini-Kolumbo Volcanic Zone represents the most active segment. The evolution of this zone has been strongly controlled by Miocene-Pliocene E-W faults and younger SW-NE structures, (Figs. 1-2a) (Fytikas et al., 1990; Papazachos and Panayotopoulos, 1993; Perissoratis, 1995). The interaction between fault systems provide a key role in facilitating magma ascent resulting in the development of a shallow magma reservoir at depths of 3-6 km beneath Santorini Island. Geophysical and seismological studies suggest that the magmatic system is closely associated with intense seismicity, frequent earthquake swarms and episodes of magma intrusion (Druitt et al., 1989; Fytikas et al., 1990; Newman et al., 2012; Papazachos et al., 2025; Hufstetler et al., 2025; Lomax et al., 2025) (Figs. 1-2).

Long-term geochemical monitoring in AEP has shown that local geological conditions (lithology, permeability contrasts, and active fault proximity) strongly control the detectability of seismic precursors. The radon anomalies and groundwater chemical shifts (İnan et al., 2010; Yakupoğlu et al., 2025) have been linked to crustal stress changes, but site-specific responses are modulated by the heterogeneity of the fault network and the presence of microplate boundaries (Nyst and Thatcher, 2004; Reilinger et al., 2006).

3. Methods and Instruments

3.1 Cumulative moment of the February-March 2025 Santorini EQ swarm

The cumulative seismic moment released during the February-March 2025 Santorini earthquake swarm was quantified by summing the scalar seismic moment (M_0) of individual events (Fig. 2). Scalar seismic moments (M_0, in Nm) were calculated for each earthquake using the classical moment-magnitude relationship:

$$Mw = (\log_{10}(M_0) - 9.1)/1.5 \qquad \text{(Kanamori, 1977; Hanks and Kanamori, 1979)} \tag{1}$$

The individual seismic moments were then summed to obtain the total cumulative moment of the swarm. For descriptive purposes only, the cumulative moment was formally converted back into an equivalent moment magnitude (Mw), representing the integrated seismic moment release of the entire sequence. This equivalent magnitude should not be interpreted as implying dynamic or mechanical equivalence to a single impulsive earthquake rupture. In addition to moment summation, the radiated seismic energy (E, in joules) was estimated independently using the empirical magnitude-energy relation

$$\log_{10}(E) = 1.5 \cdot Mw + 4.8 \qquad \text{(Kanamori, 1977; Choy and Boatwright, 1995)} \tag{2}$$

The moment-based and energy-based estimates were used to provide a consistency check on the total seismic budget of the swarm, rather than as independent constraints on rupture dynamics. The estimated cumulative moment and radiated energy place the overall seismic budget of the swarm within the magnitude range commonly attributed to a Mw ~6.1-6.2 earthquake. This comparison refers exclusively to the cumulative energy or moment release and does not account for the temporal distribution, spatial extent, or stress-transfer characteristics unique to swarm-type seismicity. The resulting estimates are consistent with recent independent assessments based on waveform modeling and focal-mechanism clustering, which reported a total radiated energy on the order of 1×10^{14} joules for the same sequence (Toker et al., 2025). All related displays are present on Figs. 2c-d.

3.2 Evaluation of hydrogeochemical anomalies in terms of distance and magnitude

To place the observed hydrogeochemical variations in a broader seismotectonic context, previously published empirical scaling relations between earthquake magnitude and the maximum reported distance of hydrogeochemical or geophysical anomalies were considered (Dobrovolsky et al., 1979; Bowman et al., 1998; Martinelli and Tamburello, 2020). These relations were originally developed for single mainshock events and express statistical envelopes of anomaly occurrence as a function of earthquake magnitude, rather than deterministic prediction

limits. In these relations, D represents the distance between earthquake epicenter to the spring location, Mw is the moment magnitude of the event.

$$D = 10^{\wedge}(0.43 \cdot \mathrm{Mw}) \tag{3}$$

$$\log \mathrm{D} = 0.5 \cdot \mathrm{Mw} \tag{4}$$

$$\mathrm{D} = 10^{\wedge}(0.28 \cdot \mathrm{Mw} + 0.25) \tag{5}$$

For a reference magnitude of Mw ≈ 6.1, adopted here solely as a formal representation of the cumulative seismic moment or energy budget of the Santorini swarm, these relations yield characteristic distance ranges spanning from ~90 km to ~1100 km. Within this conceptual framework, the Naz-01 spring, located approximately 280 km from the central area of swarm activity, falls within or near the broad distance ranges reported by these empirical models (Fig. 1; Nyst and Thatcher, 2004; Reilinger et al., 2006). This comparison does not imply a direct causal relationship, but rather provides a contextual assessment of whether the observed anomaly occurs at distances commonly reported in previous precursor studies (see references in the introduction). It should be emphasized that the applicability of such relations to swarm-type seismicity remains uncertain, as swarm activity differs fundamentally from single large earthquakes in terms of temporal evolution, spatial distribution, and stress transfer. Therefore, the empirical distances presented here are used only as qualitative reference bounds and are not interpreted as predictive thresholds.

3.3 Water Samples and Electrical Conductivity (EC) Measurements

Commercially-bottled spring water samples were obtained in polyethylene bottles and brought to İstanbul Technical University. 42 Spring water samples on Naz-01 cover April 2023 to July 2025 (28 months) in the AEP region (Figs. 1-3). Additionally, 41 spring water samples from both Boz-01 and Çine-01 provided to cover the duration between April 2024 to Jan 2025 and April 2023 to February 2025 respectively (Figs. 1-3). EC measurements were conducted by using a pen-type AZ8361 hand probe (error rate is ~1-3 µS/cm) within the first month after the collection. All measurements were conducted at room temperature for standardization in measurements. Prior to each EC measurement probe was cleaned and rinsed with deionized water (~18 MΩ). All EC results were plotted and correlated with rainfall variations for spring water region (Fig. 3). Consequently, all the samples of Naz-01 were conducted for major ion analysis using ion chromatography (IC) (Fig. 4). The results of the analyses are provided in Tables 1-2.

3.4 Ion Chromatography (IC) Analysis

Major ion contents of samples from spring water location (Naz-01) were analyzed by IC as discussed by Zeyrek et al. (2010). All 42 samples are analyzed IC right only few days after the EC measurements. Samples were filtered at 0.45 µm and split into two portions before the analyses. Sodium carbonate and methane-sulfonic acid were used as eluents for anion and cations, respectively. Ion chromatography instrument (Dionex ICS-1000) was used for analyses thus, DIONEX certified reference standards were used for calibration. Preparation of all eluents were done with deionized water (~18 MΩ). Three subsequent measurements were executed for each sample within the 5% uncertainty interval. IC analysis results were successively plotted and interpreted for further discussion (Fig. 4). The results of the analyses are presented in Table 1.

In order to provide a better understanding of the changes in between ion distributions, Principal Component Analysis (PCA) has been applied to the IC results by using Past4.03 software. PCA is a statistical technique that identifies correlation relationships within data, allowing the dimensionality of a dataset to be reduced while keeping the structural information. It has been effectively used to interpret the hydrogeochemical characteristics of similar approaches (Nicholson, 1993; Boschetti et al., 2003; Awaleh et al., 2020; Barbieri et al., 2021). Given the relatively low

sampling frequency of the dataset, PCA was preferred over high-resolution time-series approaches (e.g., lag-correlation or event-based statistical testing), as the available temporal resolution does not allow statistically robust treatment.

4. Results

4.1 Cumulative earthquake magnitude of the Santorini EQ swarm

Between February-March 2025, the Santorini region experienced an intense seismic swarm comprising 879 earthquakes with magnitudes Mw >3.0, and more than 2,000 events in total when smaller magnitudes are included (Toker et al., 2025) (Figs. 2a-b). Despite the absence of a single large mainshock (the maximum recorded was Mw 5.3),

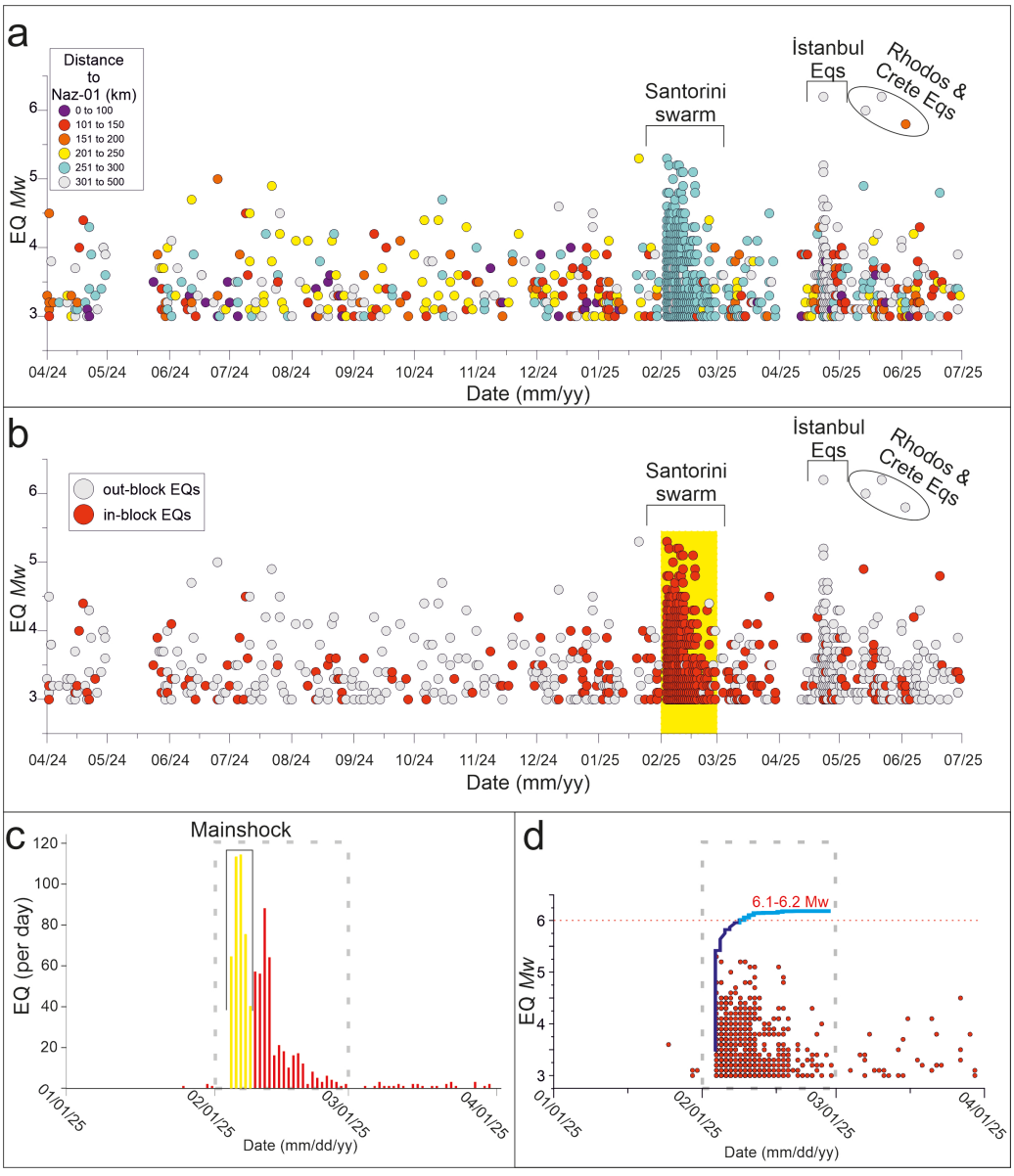

Figure 2. Distributions of earthquakes within the 350 km radius of spring water (Naz-01). (a) Between April 2024 to July 2025 distribution of Mw and distances of EQs around the region. (b) Same EQ distribution according to the locations of the microplate (see dark gray colored lines in Fig. 1 and Nyst and Thatcher, 2004; Reilinger et al., 2006). (c) close up section of the histogram profiles showing the number of EQs occurred (>Mw 3.0) each day during February-March Santorini EQs swarm. d) Cumulative moment distribution of the Santorini EQs showing the total energy release calculated as single 6.1-6.2 Mw EQ (see related references in the text).

the swarm exhibited strong spatial and temporal clustering over a ~40-day period, however the main shocks occurred in the first 5 days (Feb 2nd to 5th, total of ~400 earthquakes exceeding M > 3.0) indicative of a coherent stress-release episode. Given this collective behavior, the sequence is treated as a compound seismic source and applied a cumulative moment summation approach to quantify the total energy released as if it originated from a single equivalent earthquake (Figs. 2c-d). Using the total radiated energy reported by Toker et al. (2025), estimated at $E = 1 \times 10^{14}$ joules, the corresponding moment magnitude was calculated as Mw 6.1-6.2 based on the energy-magnitude relationship (relations 1-2). This value aligns with the energy-equivalence proposed and is also illustrated in Fig. 2c-d of this study (see Fig. 1d in Toker et al., 2025; Triantafyllou et al., 2025).

This result suggests that, when integrated over time and space, the swarm effectively matches the total energy release of a single moderate-to-strong earthquake with a magnitude of Mw ~6.1 (Fig. 2d). This equivalence may be useful to suggest that the empirical models can be utilized for individual events of similar size. The cumulative moment progression (Fig. 2) further reveals a steady, swarm-like dynamic rather than a classical mainshock-aftershock pattern, reinforcing the rationale for collapsing the sequence into a single-event framework (Figs. 1-2). This equivalence refers solely to the *integrated seismic moment/energy budget* and does not imply dynamic or mechanical equivalence to a single mainshock (Figs. 1-3).

4.2 EC measurements of Spring water samples

The Santorini earthquake cluster occurred time between February-March 2025 (Figs. 1-3). In statistical sense, anomalies are measured by the exceeding sample points of the background nominal level of EC prior to the event timeline. In each spring water graph, stable trends are accounted for background level and mean and standard deviations are calculated on these samples. Exceeding EC points are defined as the anomalies. This approach is effectively used in several similar studies (İnan et al., 2008, 2012b, 2024; Skelton et al., 2014; Yakupoğlu et al., 2025; Li et al., 2026) EC record of Çine-01 covers 23-month long timeline. Results show a stable trend within the years, EC values diverse between 100-70 µS/cm only one sample exceed the 2σ threshold (Figs. 1-3a) (Table 2). Similar to Çine-01, Boz-01 spring water record covers the time between 9 months showing only the pre-earthquake stage of the Santorini events (Figs. 1-3b). EC records show a stable trend (180-195 µS/cm) within the 2σ threshold (Table 2). EC record of the spring water Naz-01 located near Nazilli, Türkiye (Figs. 1-3c). EC is plotted with rainfall of the Nazilli region (dark blue histogram bars in Fig. 3c) (Table 1). All earthquakes (Mw ≥3.0) that occurred between same timeline are also plotted subsequently (Figs. 3d-f).

EC records of Naz-01 spring water samples covers the time interval May 2023 to June 2025. Two distinct anomalies are present in between Oct 2023 to Dec 2023 and June 2024 to Jan 2025 (Fig. 3c). Rest of the data within the mean values of the EC, is considered as background samples. The mean value of these samples has a mean of 109 µS/cm and have 9 µS/cm of standard deviation (Figs. 3c-4a and Table 1). These anomalies are considered to related with the 27 Jan 2024 Kuşadası 5.0 Mw EQ and Feb 2025 Santorini EQs respectively. Rainfall around the Nazilli region shows seasonal variations during the 28-month long timeline (Fig. 3c). Each year, end of spring and winter seasons have rainfall (10-15 mm/day) however, summer and fall seasons rather seem arid.

Table 1. EC and IC results of Naz-01. Mean and two standard deviation (2σ) values of the all dataset are indicated in parenthesis of each column respectively. Data are plotted in Figs. 3-4.

Date (mm/dd/yy)	EC (µS/cm) (109, 25)	Cl^- (mg/L) (2.36, 0.42)	SO_4^{-2} (mg/L) (16.58, 4.88)	Na^+ (mg/L) (5.02, 1.17)	K^+ (mg/L) (1.41, 0.35)	Mg^{+2} (mg/L) (3.25, 1.33)	Ca^{+2} (mg/L) (10.39, 2.84)
05/02/23	72	1.56	8.08	5.86	1.66	2.50	4.65
10/02/23	95	2.75	12.97	6.62	0.83	2.49	9.37
10/04/23	91	2.38	14.58	4.78	1.80	3.54	6.38
10/12/23	130	3.05	21.55	6.99	2.05	5.78	10.17
11/20/23	125	3.10	22.58	5.18	1.90	5.05	10.36

Date (mm/dd/yy)	EC (µS/cm) (109, 25)	Cl^- (mg/L) (2.36, 0.42)	SO_4^{-2} (mg/L) (16.58, 4.88)	Na^+ (mg/L) (5.02, 1.17)	K^+ (mg/L) (1.41, 0.35)	Mg^{+2} (mg/L) (3.25, 1.33)	Ca^{+2} (mg/L) (10.39, 2.84)
11/21/23	132	3.16	23.95	5.50	1.97	5.54	9.95
11/23/23	126	2.94	20.70	6.86	1.97	5.55	9.98
12/05/23	143	3.57	24.66	7.67	2.13	6.49	11.34
12/09/23	85	2.07	12.57	5.40	1.51	2.93	6.75
01/04/24	115	2.59	16.86	6.51	1.84	4.43	8.27
01/05/24	101	2.62	17.75	4.48	1.64	3.62	8.51
02/08/24	99	2.55	18.02	3.23	1.03	2.10	10.71
02/16/24	100	2.41	19.18	3.17	0.98	2.07	10.63
04/19/24	84	1.94	10.39	4.40	1.06	1.89	11.38
04/29/24	85	2.19	12.00	4.16	1.44	2.42	7.04
05/10/24	86	2.20	11.88	4.22	1.39	2.44	7.26
05/31/24	96	2.36	13.54	4.27	1.40	2.69	8.43
07/01/24	82	2.03	9.66	6.32	1.70	2.75	5.36
08/16/24	139	2.23	17.36	5.60	1.52	4.44	14.81
08/20/24	100	2.91	14.72	5.21	0.88	2.37	8.62
08/23/24	132	2.23	17.05	4.41	1.31	3.33	10.45
08/24/24	101	2.84	12.89	6.83	0.86	2.47	9.17
09/02/24	142	2.30	18.15	4.92	1.50	3.78	12.48
09/06/24	139	2.22	17.92	5.13	1.45	3.93	12.84
09/09/24	139	2.37	17.21	5.28	1.50	3.95	13.35
09/24/24	150	2.43	18.62	5.75	1.68	4.49	14.85
10/15/24	152	2.41	18.83	6.03	1.60	4.70	15.73
10/23/24	173	2.61	30.07	7.23	1.74	5.50	17.50
11/08/24	154	2.42	19.73	6.15	1.64	4.83	16.49
01/06/25	130	2.36	24.57	5.13	1.45	3.14	14.35
01/21/25	95	2.00	20.77	3.89	1.35	2.09	10.12
01/24/25	95	1.95	17.91	4.16	1.38	2.33	10.32
02/14/25	97	1.83	11.87	4.64	1.22	2.58	9.79
03/03/25	86	2.12	11.95	4.14	1.27	1.77	9.21
03/04/25	85	2.18	12.18	3.83	1.11	1.61	9.15
03/17/25	102	2.42	21.99	4.05	1.22	2.05	11.07
04/29/25	79	2.15	11.75	3.80	0.98	1.43	8.24
05/15/25	80	2.14	10.86	3.90	0.95	1.47	8.40
05/21/25	78	1.68	10.38	3.31	0.88	1.80	8.35
06/09/25	102	2.56	22.26	4.20	1.05	1.97	10.93
06/24/25	104	1.67	13.16	3.72	1.05	3.02	11.65
07/05/25	108	1.66	13.19	3.79	1.12	3.19	12.05

Table 2. EC results of the Çine-01 and Boz-01 spring waters. Mean and two standard deviation (2σ) values are indicated in parenthesis of each column respectively. Data are plotted in Fig. 3.

Çine-01		Boz-01	
Date (mm/dd/yy)	EC (µS/cm) (89.95, 10.01)	Date (mm/dd/yy)	EC (µS/cm) (187.72, 2.46)
04/18/23	90	01/15/24	189
05/07/23	70	02/15/24	185
07/23/23	102	03/08/24	188
08/04/23	102	03/14/24	188
08/31/23	87	04/01/24	188
09/01/23	88	04/20/24	190
11/07/23	89	05/15/24	190
12/14/23	53	06/04/24	191
12/15/23	88	06/15/24	189
12/28/23	89	06/20/24	189
01/08/24	93	07/19/24	185
02/10/24	97	08/07/24	186
03/07/24	98	08/08/24	188
03/11/24	96	08/17/24	181
08/11/24	95	09/07/24	185
08/30/24	90	09/14/24	189
09/03/24	91	09/19/24	187
09/21/24	92	11/14/24	191
09/28/24	89		
10/11/24	92		
10/14/24	90		
10/26/24	92		
02/03/25	96		

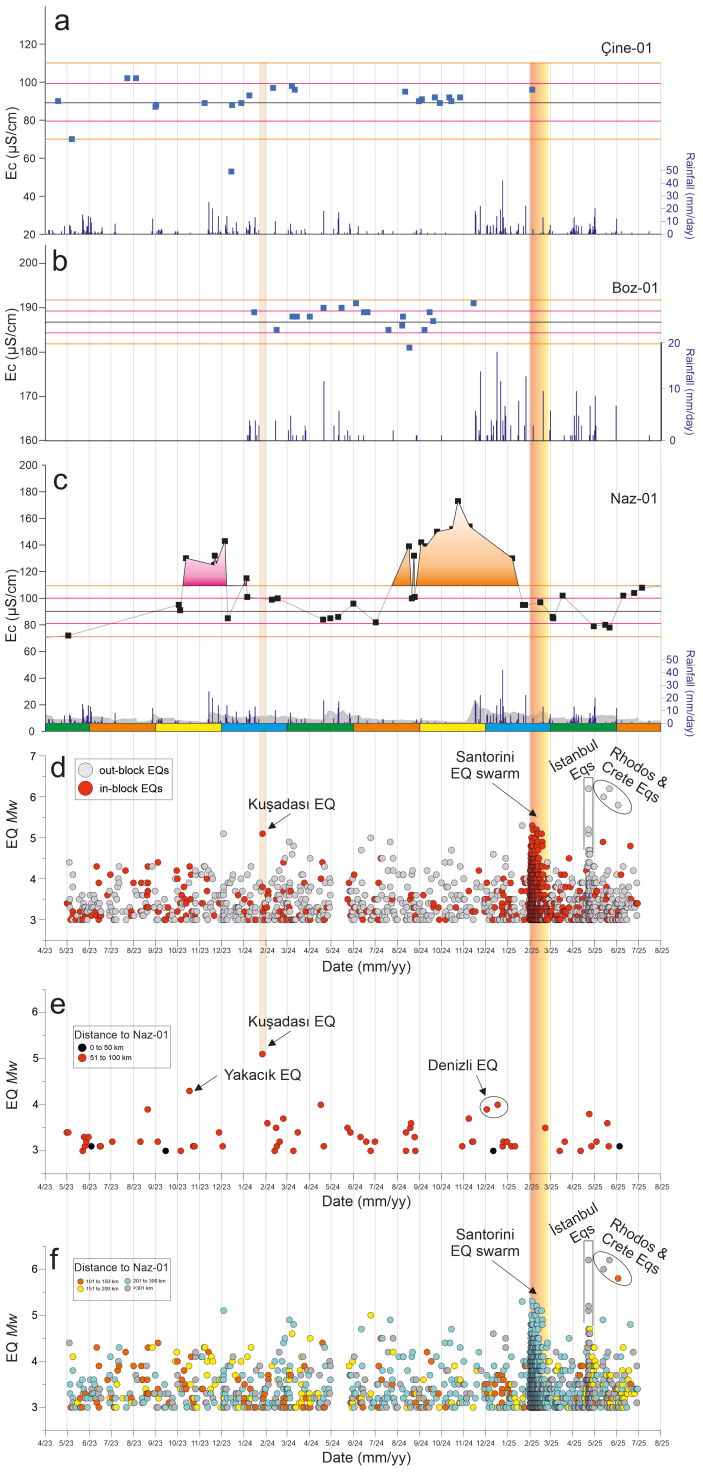

Figure 3. (a-c) EC results of the samples obtained from commercially bottled spring water in the AEP (Çine-01, Boz-01 and Naz-01 respectively). Small rectangles represent EC samples. Horizontal gray dashed lines within the EC profiles show the mean (black) and standard deviations (σ is magenta and 2σ is orange) calculated according to the background samples (see section 4.2). Dark blue histograms display daily rainfall in the area of each spring water location (https://www.meteoblue.com/tr/hava/historyclimate/weatherarchive). Seasons (spring, summer, fall and winter are placed as green, orange, yellow and blue respectively. Vertical boxes represent the time of the Kuşadası EQ and Santorini EQs respectively. (d) EQ distribution showing the in-block and out-block locations according to the microplate boundaries (see Fig. 1 and Nyst and Thatcher, 2004; Reilinger et al., 2006). (e-f) EQ distribution showing the Mw and distances of each event to the spring water Naz-01. Note that, Kuşadası event, Santorini events, Rhodes and Crete events and Silivri-İstanbul events are especially indicated (see also Fig. 1). Apr 2023 to June 2024 dataset is taken from Yakupoğlu et al. (2025).

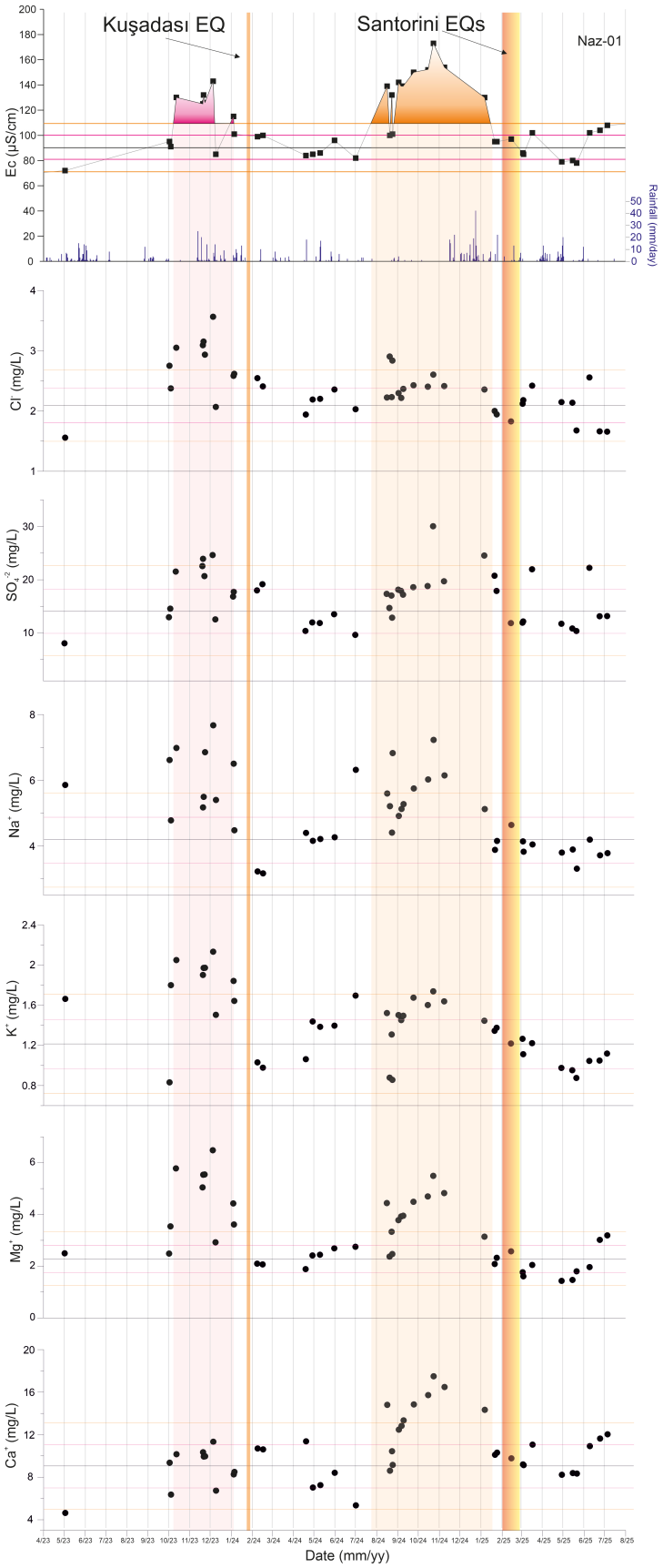

Figure 4. EC and IC (Cl^-, $SO4^{-2}$, Na^+, K^+, Mg^+ and Ca^+) results of the water samples obtained from spring water in the Nazilli region (Naz-01). Vertical boxes represent the Kuşadası EQ (27 Jan 2024) and Santorini events (Feb-March 2025) respectively. Horizontal lines represent the mean (black) and standard deviations (σ is yellow and 2σ is orange) respectively. Dashed areas illuminate the anomalous samples timeline.

4.3 IC measurements of Naz-01

IC records of the spring water Naz-01 have positively correlated trend as EC values over in all ions of the 28 months record. An apparent increase in water EC starting in Oct 2023 is also can be traced with the increase in ion concentrations are based on Cl^- (2 to 3.5 mg/L), Na^+ (4.7 to 7.6 mg/L) K^+ (1.4 to 2.2 mg/L), Mg^{+2} (3 to 6.2 mg/L). However, both SO_4^{-2} (14 to 25 mg/L) and Ca^{+2} (6 to 11.5 mg/L) have stable trends during this period. Moreover, second anomaly at the Naz-01 which occurred at the beginning of June 2024, is accompanied with SO_4^{-2} (10 to 30 mg/L), Na^+(4 to 7.2 mg/L) Mg^{+2} (2 to 5.6 mg/L) and Ca^{+2} (8 to 17.2 mg/L) whereas Cl^- (2 to 2.8 mg/L), K^+ (1.1 to 1.7 mg/L) are not displaying similar trend with EC profile of Naz-01 (Table 1, Fig. 4).

In order to evaluate and compare the distinct EC anomalies occurred in Oct 2023 and June 2024 in Naz-01, PCA analyses has been established on both anomalous samples and the background samples (see Figs. 3-4). Oct 2023 anomaly occurred prior to the Kuşadası EQ (27 Jan 2024) and two sample clusters are obtaining from the analysis. First cluster contains Cl^-, SO_4^{-2} and Ca^{+2} showing a positive correlation whereas second cluster is composed of K^+, Mg^{+2} and Na^+ with a positive correlation with each other (Fig. 5). In EC profile of Naz-01, second anomaly starting from June 2024 is considered to be related with Santorini EQ event thus, SO_4^{-2}, Mg^{+2}, Ca^{+2} form a cluster at the 1st quadrant of the analysis (Fig. 5). However, rest of the ion correlations are scattered along the 2nd and 4th quadrants. The non-anomalous samples which represents the background level of the spring water shows two cross correlated cluster correlations. In these samples, SO_4^{-2} and Cl^- is negatively correlated with Mg^{+2} thus, K^+ and Na^+ are also negatively correlated with Ca^{+2} distribution (Fig. 5). Although PCA clearly distinguishes anomalous and background geochemical signatures, the temporal resolution of the dataset does not permit a statistically robust time-series evaluation of lag relationships between hydrogeochemical variability and seismic events.

5. Discussion

5.1 Possible Mechanisms Leading to springwater geochemical anomalies

The hydrogeochemical variations observed in the monitored springs are likely governed by a combination of hydrological and geochemical processes. Seasonal variability, together with fluctuations in rainfall amount and distribution, exerts a primary control on recharge dynamics, dilution effects, and water-rock interaction within the aquifer system. Furthermore, temporal variations in the relative contributions of meteoric and deep groundwater, enhanced inputs from deeper hydrothermal fluids, and changes along hydraulic pathways may lead to measurable modifications in water chemistry. However, these variations may also be driven by earthquake-related processes, as seismic stress and strain changes have the potential to disturb subsurface fluid circulation, modify hydraulic connectivity, and enhance mixing between shallow and deep fluid reservoirs.

Seasonal variability can be traced by the EC anomalies that occur within the same time periods over the years. In Fig. 3, only Naz-01 has a distinct anomalous trend within the 28-month long record. Boz-01 and Çine-01 has no distinct anomalies or spikes, reason for that will be covered in Section 5.2 extensively. For the record of Naz-01, EC anomalies occur between Oct 2023 to Jan 2024 and Aug 2024 to Jan 2025. Timing of the anomalies are not entirely conformable with each other in terms of duration and amplitude. Thus, chemical composition of these anomalies which are depicted by IC results indicates variability between anomalous seasons due to increment of different ion contents (Fig. 4). The first anomaly (Oct 2023 to Jan 2024) is controlled by increase in Cl^-, K^+, Mg^{+2} (Fig. 4). The latter (Aug 2024 to Jan 2025) is dominated bySO_4^{-2}, Na^+, Ca^{+2} respectively (Fig. 4).

Both anomalies (IC results) within the same spring is also conducted in PCA analysis and radar diagram in order to show the differentiation of the characteristics of the anomalies. Given the 28-month long EC and IC record at least 2 yearlong seasonal variations have been scanned (Fig. 5). PCA distribution of the both anomalies differ in terms of ion content (Figs. 5a-b). EC anomalies occur between Oct 2023 to Jan 2024 and Aug 2024 to Jan 2025 display two sets of ion clusters are present themselves in different compositions. Cl^-, K^+, Ca^{+2} ratios show different geochemical settings of each anomaly as well as forms different clusters in the radar diagram (Fig. 5). Therefore, they could not be related with seasonal variability when considered as each anomaly is caused by unique ion trends as well as have different amplitudes and periods of EC and IC (Figs. 3-5).

Rainfall could be a reason for providing and/or prevent trends of EC by diluting the composition of the spring waters. If the aquifer system is somehow connected to the infiltration pathways EC of the spring water could be

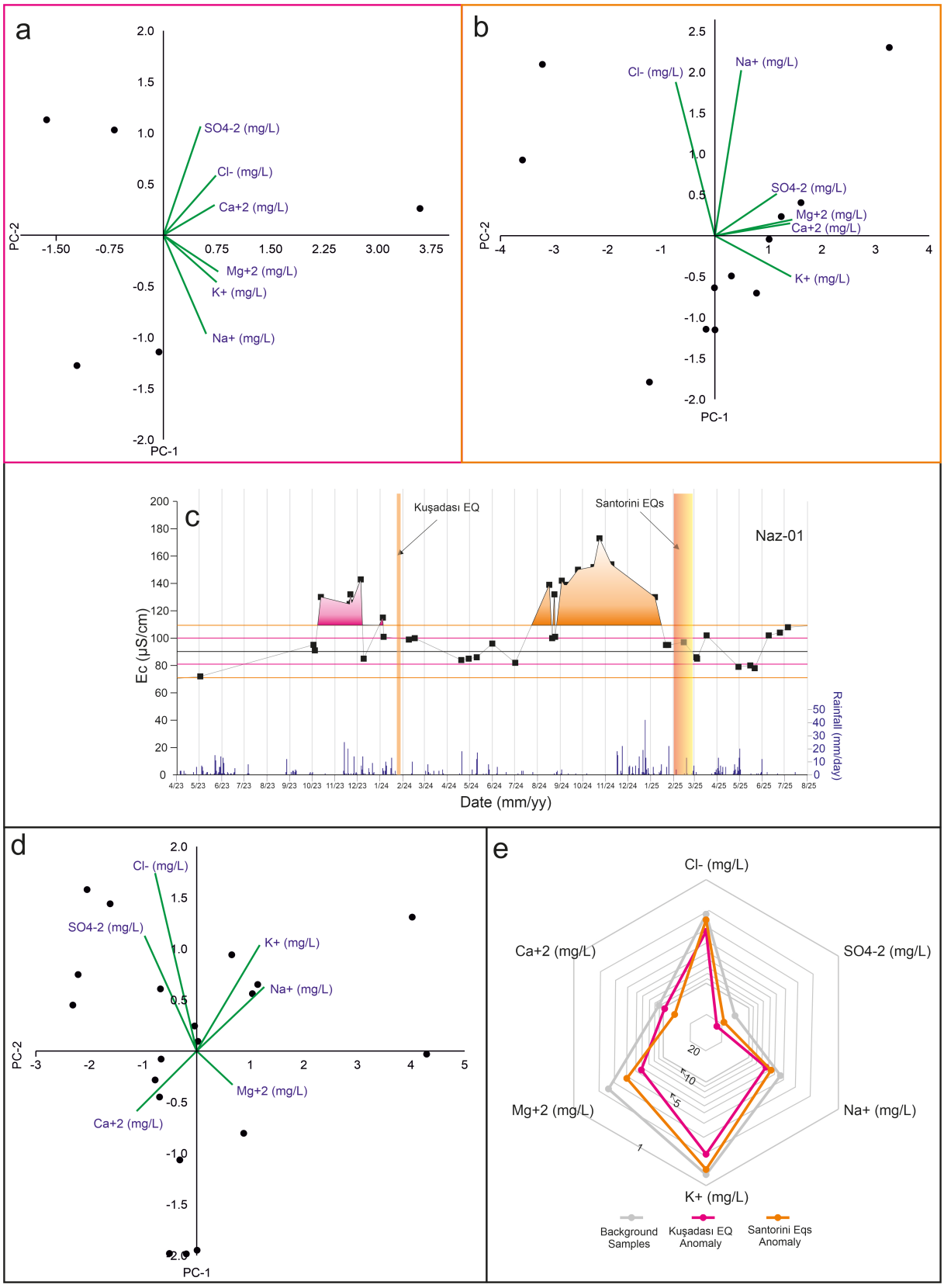

Figure 5. PCA analysis on IC results of Naz-01 spring. (a-b) Distribution and correlation factors of each ion of the anomaly before the Kuşadası EQ (Oct 2023-Dec 2023) and Santorini events (Aug 2024-Jan 2025) respectively displaying two distinct clusters of ions loading factors. (c) EC distribution of Naz-01. (d) Distribution of ions within the background samples showing dispense correlation. (e) Radar diagram of the IC averages of the background samples and samples of anomalous periods showing the differentiation of the clusters for different periods. Note that the concentrations increase from the periphery to the center.

suppressed. Therefore, correlation between rainfall and the EC profiles to demonstrate the possible relations. In this study, each EC trends carefully correlated with the rainfall of the vicinity of the region (Fig. 3; blue histograms). In terms of Naz-01, rainfall and its moving average (for 30 days) is placed subsequently to should be taken into consideration when correlating EC result.

Rainfall distribution displays spring-winter accumulation in the Nazilli region. Generally, summer-fall seasons are lack of precipitation (Fig. 3c). Peak of the rainfall occurs at the termination of fall or the beginning of winter. During December to February, there are alternating rainy weeks that accumulates (mean of 10-25 mm/day) contribution. During the spring seasons, 10-15 mm/day of rain is observed in the Nazilli region (Fig. 3c). The occurrence of the rainy periods does not coincide with the onset of the anomalies which shows the initiation of the anomalies could not be related with the rainfall. However, in both anomalous periods (Oct 2023 to Jan 2024 and Aug 2024 to Jan 2025) termination of these anomalies coincide with the precipitation during the winter season that could be diluting the spring water composition and attenuate the EC increments (Fig. 3c).

The rest of the possible controls over the EC anomalies could be related with local event due to contribution of deeper hydrothermal fluids, meteoric groundwater mixing. In order to show these parameter's contribution temperature of the spring water during the sampling and barometric pressure measurements are needed. However, there is no such data collected during this research. The absence of multiparametric observations (e.g., piezometric levels, temperature, discharge, isotopic tracers) limits the ability to exclude alternative hydrogeological drivers.

Last of the possible mechanisms that can alter the geochemical composition of the spring waters is earthquakes. Especially, prior to seismic shaking due to stress distribution changes water-rock interaction within the aquifer system can disturbed and changes along hydraulic pathways may occur which lead to measurable modifications in water chemistry. This study provides two chemically-unique anomalous periods during over two years of spring water record that could be appointed as precursory geochemical changes of the Kuşadası and Santorini earthquakes when eliminating other possible mechanisms; within the constraints of the available dataset, these periods are temporally consistent with the respective earthquakes and provide evidence for stress-induced fluid redistribution, although this relationship cannot be independently constrained by the available parameters. (Figs. 1-3) (see also Fig. 2 in Yakupoğlu et al., 2025).

The February-March 2025 Santorini earthquake swarm presents a compelling case study for evaluating long-range hydrogeochemical responses to distributed, low-to-moderate magnitude seismicity. Over 2,700 earthquakes were recorded around Santorini Island and its vicinity (Toker et al., 2025; Triantafyllou et al., 2025). This cumulative energy perspective provides a basis for interpreting the swarm as a compound stress-inducing phenomenon capable of generating pre-seismic hydrogeochemical anomalies (Figs. 2-3). Conventional empirical models which assume that the crust is isotropic and homogeneous, typically constrain the detection radii of hydrogeochemical precursors to about 50-100 km for Mw 4.0 events (Dobrovolsky et al., 1979; Bowman et al., 1998; Martinelli and Tamburello, 2020). These models are based on simplified homogenous and isotropic crust assumptions and do not explicitly incorporate heterogeneous permeability structures or fluid-driven processes. However, the anomalous period of Aug 2024 to Jan 2025 was recorded at the Naz-01 spring, located ~280-300 km northeast of the Santorini epicentral zone (Figs. 1-3). Based on empirical range estimations, if each earthquake in the swarm were treated independently, none would be expected to induce observable hydrogeochemical effects at such a distance (see relations 1-3 in section 3.4). In contrast, when the swarm is interpreted as a cumulative seismic source (Fig. 2d), its effective hydrogeochemical impact radius which estimated between approximately between 90-1000 km for Mw 6.1-6.2 events, comfortably covers the spring site Naz-01 (Fig. 1). Similar approach has been conducted for 27 Jan 2024 Kuşadası EQ (5.0 Mw). Distance between this event and the Naz-01 is approximately 120 km which is within the hydrogeochemical anomaly radius (Dobrovolsky et al., 1979). The anomaly was characterized primarily by elevated electrical conductivity (EC) values, accompanied by increased concentrations of major ions, beginning approximately 3 months before the Kuşadası EQ (Fig. 3c). This early geochemical anomaly likely reflects regional stress redistribution across the broader Aegean domain, including the Menderes Fault System, and may indicate fluid migration along stress-activated aquifer pathways (İnan et al., 2024; Yakupoğlu et al., 2025). This mechanism is supported by ion-specific evidence, concurrent increases in EC, Cl^-, SO_4^{2-}, Na^+, K^+, Mg^{2+}, and Ca^{2+} concentrations at Naz-01 in each Oct 2023 to Jan 2024 period prior to Kuşadası event (Figs. 1-3). Similar behavior of the EC an IC profiles of Naz-01 has been detected 6-7 months before the Santorini events (Feb-March 2025) which suggest mobilization of deeper, mineral-rich fluids during the preparatory phase of the Santorini earthquakes (Fig. 4). However, even the empirical approaches cannot indicate such long periods of anomalies (Sultankhodhaev, 1984) which suggests anomaly duration of several weeks for Kuşadası and Santorini events. These empirical relationships

are based on simplified, homogeneous and isotropic crustal assumptions and may not adequately represent heterogeneous fault-hydrogeological systems. Therefore, the observed precursor durations are not necessarily expected to conform strictly to the time ranges predicted by such magnitude-distance scaling models. Therefore, previous examples report that precursor durations from weeks to several months, including a few months before $M > 5$ earthquakes (Skelton et al., 2014) and several months prior to the 1995 Kobe earthquake (Hartmann and Levy, 2006) and up to 6 months (İnan et al., 2024) while 20-90 day lead times were observed before Mw~7 events (Bella et al., 1998). Thus, multi-month hydrogeochemical anomalies are within the documented range and may exceed empirical magnitude-distance expectations. This could be related with the influence of smaller but closer earthquakes occurred around the vicinity of the regions. For this study, as it focused on Fig. 3e, in the Menderes fault zone, there are couples of smaller events (Denizli EQs) that occurred within the anomalous stage of Aug 2024 to Jan 2025 except from the Santorini earthquakes. Although these smaller events cannot produce the months long anomalies themselves, these events could only be an auxiliary effect that amplify the anomaly duration when the distance of the Santorini events is considered as distant for such long and strong anomaly (Figs. 1-3). Such secondary seismicity may further prolong permeability evolution and groundwater mixing, extending the observed anomaly beyond predictions based exclusively on the proposed Santorini events. Comparable multi-month hydrogeochemical variability has been documented in extensional and swarm-related settings (Wakita et al., 1988; Barberio et al., 2017; Luque-Espinar and Mateos, 2023), indicating that prolonged precursor phases are not unprecedented in fluid-controlled systems. In such tectonic environments, precursor behavior is strongly site-dependent and influenced by cumulative stress history and progressive permeability evolution within fractured aquifers (Wakita et al., 1988). Pre-seismic dilatation and fault-controlled fluid upwelling in extensional regimes may generate significant geochemical deviations lasting several months (Barberio et al., 2017; Luque-Espinar and Mateos, 2023). Accordingly, extended anomaly durations may reflect gradual stress accumulation and fluid redistribution rather than short-lived rupture effects alone.

These observations are consistent with previous studies in the region. İnan et al. (2010) suggest that, in the Gediz Basin near Manisa that located at east of the Naz-01 site, sequential earthquakes of Mw >4.0 were associated with distinct EC anomalies. Moreover, in Yakupoğlu et al. (2025) the anomalous period of Oct 2023 to Jan 2024 is investigated in terms of fault zone permeability and pore pressure, promoting fluid redistribution and intensified water-rock interactions (Fig. 6) (Sibson, 1992; Rojstaczer et al., 1995; Çetin, 1999; Federico et al., 2008). The Nazilli region is lack of smaller magnitude of earthquakes when compared the adjacent section of the Menderes Fault (see Fig. 1 and see Fig. 1 in İnan et al., 2010). This makes the region suitable position for hydrogeochemical research and put the region forward as hypersensitive for such responses (İnan et al., 2010).

5.2 Structural Alignment as a Key Factor in geochemical Monitoring

While numerous studies have reported hydrogeochemical precursors to seismic activity, such signals are not universally observed. This inconsistency implies that epicentral proximity alone is insufficient; structural and geological context plays a fundamental role. İnan et al. (2010), İnan et al. (2012b) and Li et al. (2026) initially emphasized that the absence of anomalies in some springs (even when close to earthquake sources) can be explained by structural decoupling between the seismic source and the observation site. If the earthquake and the spring are located on different tectonic blocks, stress transmission pathways may be effectively attenuated. In İnan et al. (2012b), They detected the hydrogeochemical imprint on the Simav earthquake (Mw 6.0 at 19 May 2011) on a distant monitoring site rather closer sites did not provide a distinct anomaly. Accordingly, they provided the relevance of geographic position of the monitoring site which must be related with the tectonic domain (see Fig. 4 in İnan et al., 2012b). Another interpretation on the structural alignment has been documented in Tibetan plateau where Lancang-Gengma fault system is monitored by meteoric deep waters from various locations (Li et al., 2026). The observations indicate that only springs structurally aligned with active faults and hydraulically connected to deep circulation pathways exhibit clear seismic-related hydrogeochemical anomalies, whereas other springs remain unresponsive, emphasizing the critical role of monitoring site location rather than earthquake occurrence alone.

In this study, Naz-01 clearly show a distinct anomaly before the Santorini events however, both Çine-01 and Boz-01 do not display such case. This contrast indicates that the observed response at Naz-01 spring is not spatially uniform across the monitoring network and may reflect site-specific structural controls. The one of the possible cause can be that Boz-01 located on a different tectonic block (Figs. 1-6) than Naz-01 makes it conformable with

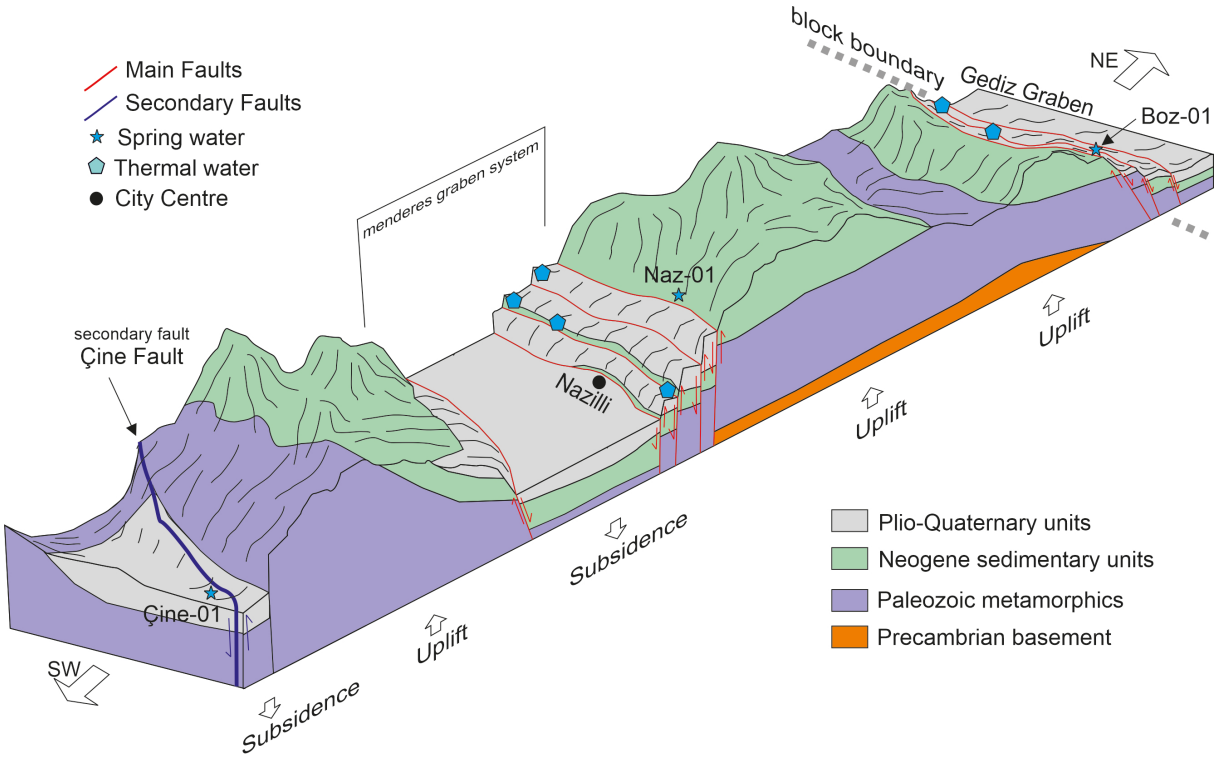

Figure 6. Geological and tectonic illustration on vicinity of the spring water regions. Orientation and the location of the cross section is shown at Fig. 1. Note that, spring waters are located on different faults. Naz-01 is located on Menderes fault, Çine-01 is located on a secondary fault and Boz-01 is located on Gediz fault which is within adjacent block. Modified and interpreted based on İnan et al. (2010).

the structural alignment as proposed by (İnan et al., 2010; Yakupoğlu et al., 2025; Li et al., 2026) Interestingly, Çine-01 is located on the same tectonic block as Naz-01 yet, there is no particular anomaly before the Santorini events. As it is indicated before (İnan et al., 2010, 2012b; Yakupoğlu et al., 2025) the most susceptible spring waters are generally located on the main fault zones. In our case, Çine-01 is located away from the main Menderes fault zone (Figs. 1-6). Moreover, the absence of the anomaly on Çine-01 is previously documented on the Kuşadası 5.0 earthquake in 2024 (Yakupoğlu et al., 2025) where Çine-01 did not displayed a distinct anomaly even though it was closer to the epicenter of the event (see Fig. 1 in Yakupoğlu et al., 2025). The susceptibility of the main fault zones can be integrated with the presence of thermal water sites in the vicinity of the regions. Similar implication has been proposed on Central Italy 2016-2017 seismic sequence (Barberio et al., 2017) showing the proximity of springs to thermal or hydrothermal systems likely enhances their susceptibility to seismic-related anomalies by facilitating stress-sensitive deep fluid flow. Another example is defined by Martinelli and Tamburello (2020) which demonstrated that fluid-related seismic precursors preferentially occur in areas characterized by high heat flow, shallow seismicity, and proximity to volcanic or hydrothermal systems, indicating that springs connected to such environments are more susceptible to recording stress-induced anomalies. In Figs. 1 and 6, the main Menderes fault contains several thermal water sites whereas on Çine fault there is none (see the blue pentagons on Figs. 1 and 6). This strongly suggest that presence of the fault driven fluid interaction makes the monitoring sites more susceptible to the chances of the stress distribution in the region. Similarly, Li et al. (2026) demonstrates the importance of the connectivity of the spring to the circulation pathways which could be the result of the unresponsive behavior of the Çine-01 spring. To ensure this kind of contradictory, multiple monitoring sites and years long continuity is crucial. However, the absence of comparable signals at Çine-01 and Boz-01 suggests that structural alignment alone may not be sufficient, and local hydrogeological characteristics likely modulate the sensitivity of individual springs. Another notable example is the Mw 5.0 Mudanya-Gemlik earthquake, which was geographically closer to Istanbul and Bursa than to Sapanca (see Fig. 1 in Yakupoğlu et al., 2025). Yet, no anomalies were detected in the springs of Istanbul or Bursa, whereas Sapanca which despite being more distant, exhibited a clear geochemical response (see Fig. 2 in Yakupoğlu et al., 2025). This spatial discrepancy is attributed to micro-tectonic compartmentalization

while Istanbul and Bursa lie outside the deformational block affected by the event, Sapanca lies within the same active tectonic unit (Fig. 1).

Aside from the Santorini events, this study reveals similar patterns on subsequent earthquakes that occurred in 2025. Following the Santorini swarm in first quarter of 2025, seismic activity continued in the Silivri-Istanbul and Rhodes-Crete regions. The Silivri earthquakes (~300-350 km from the Nazilli spring) (Fig. 1) occurred across several major fault systems, including the middle and southern branches of the North Anatolian Fault and the east-west-trending normal faults of the Aegean extensional regime. According to the tectonic block models of Nyst and Thatcher (2004) and Reilinger et al. (2006), these earthquakes and the Nazilli spring lie on structurally decoupled domains, explaining the absence of geochemical anomalies. Even the Rhodes-Crete earthquakes, which were closer (~100 km to Naz-01 spring water) (Figs. 1-2a) and of moderate-to-strong magnitude (Mw >5), did not elicit detectable changes in EC or IC records (Figs. 3-4). This further supports the hypothesis that structural connectivity, rather than mere proximity, governs the manifestation of hydrogeochemical precursors. The Naz-01 spring and these earthquakes are situated on separate micro-tectonic blocks (Fig. 1). These findings underscore the necessity of incorporating tectonic block configuration into the design and placement of hydrogeochemical monitoring networks. Monitoring stations must be evaluated not only by spatial distance to seismogenic sources, but also by their structural alignment within the same deformational regime to ensure accurate and meaningful precursor detection. The differential response among the monitored springs emphasizes that structural alignment is a controlling factor in precursor manifestation, with site-specific hydrogeological conditions determining the sensitivity of individual springs.

6. Conclusion

This study discusses possible precursory hydrogeochemical anomalies and compares the anomaly characteristics of a single shock event and earthquake swarm events, despite their considerable distance from the observation site. The elevated electrical conductivity and ion concentrations recorded in spring waters several months before the Santorini earthquake swarm may indicate crustal stress-induced permeability changes and the upward migration of mineral-rich fluids into distant shallow aquifers. When all possible causes of positive anomalies (seasonal variability, enrichment via rainfall infiltration, deep meteoric mixing) are considered, the findings suggest that such long-distance responses may be possible when the monitoring site is structurally connected to the seismogenic source through active fault systems within the same deformational block. In contrast, earthquakes of similar or greater magnitude, even at closer distances to the monitoring site, occurring in structurally decoupled regions (e.g., in a different tectonic block) produced no significant changes. These observations suggest that tectonic connectivity may represent a more critical factor for precursory manifestations than epicentral proximity alone within the temporal resolution limits of the dataset. The contrasting behavior among the monitored springs further indicates that hydrogeochemical responses are not regionally uniform but are modulated by structural alignment and local hydrogeological configuration. For more effective monitoring, site selection should consider both geological setting and structural alignment with potential earthquake sources, and this framework should be further tested and refined in future studies across different tectonic settings. Long-term, high-resolution, multidisciplinary observation networks including but not limited to shallow and deep-water systems, remain essential for improving the predictive capability of hydrogeochemical monitoring in complex tectonic environments.

Data availability statement. Data will be made available on request.

Acknowledgements. First, I thank Mr. Ali Cemal Emeç and Mr. Serhan Doğan Yakupoğlu for their help in collecting samples. I appreciate all the technical help that received on ion chromatography analyses from Dr. Sevde Korkut at the Istanbul Technical University MEM-TEK laboratory. I also thank the handling editor and two anonymous reviewers for their constructive reviews which greatly helped improve the manuscript. This work has been partially supported by Istanbul Technical University Scientific Research Fund (ITU BAP) project no: 46388.

References

Abbad, S., M. C. Robe, M. Bernat and V. Labed (1995). Influence of meteorological and geological parameter variables on the concentration of radon in soil gases: application to seismic forecasting in the Provence-Alpes-Cote d'Azur region, Environ. Geochim. Health, 16, 35-48.

Awaleh, M. O., T. Boschetti, A. E. Adaneh, M. A. Daoud et al. (2020). Hydrochemistry and multiisotope study of the waters from Hanlé-Gaggadé grabens (Republic of Djibouti, East African Rift System): a low-enthalpy geothermal resource from a transboundary aquifer, Geothermics, 86, 101805, doi:10.1016/j.geothermics.2020.101805.

Barberio, M. D., M. Barbieri, A. Billi, C. Doglioni et al. (2017). Hydrogeochemical changes before and during the 2016 Amatrice-Norcia seismic sequence (central Italy), Sci. Rep., 7, 11735, doi:10.1038/s41598-017-11990-8.

Barbieri, M., S. Franchini, M. D. Barberio, A. Billi et al. (2021). Changes in groundwater trace element concentrations before seismic and volcanic activities in Iceland during 2010-2018, Sci. Total Environ., 793, 148635, doi:10.1016/j.scitotenv.2021.148635.

Bella, F., P. F. Biagi, M. Caputo, E. Cozzi et al. (1998). Hydrogeochemical anomalies in Kamchatka (Russia), Phys. Chem. Earth, 23, 9-10, 921-925, doi:10.1016/S0079-1946(98)00120-7.

Boschetti, T., G. Cortecci and L. Bolognesi (2003). Chemical and isotopic compositions of the shallow groundwater system of Vulcano Island, Aeolian Archipelago, Italy: an update, Geodin. Acta, 2, 1-34.

Bowman, D. D., G. Ouillon, C. G. Sammis, A. Sornette et al. (1998). An observational test of the critical earthquake concept, J. Geophys. Res. Solid Earth, 103, B10, 24359-24372, doi:10.1029/98JB00792.

Bozkurt, E. and S. K. Mittwede (2005). Introduction: Evolution of continental extensional tectonics of western Turkey, Geodin. Acta, 18, 3-4, 153-165, doi:10.3166/ga.18.153-165.

Briole, P., A. Ganas, A. Serpetsidaki, F. Beauducel et al. (2025). Volcano-tectonic interaction at Santorini, The crisis of February 2025, Constraints from geodesy, Geophys. J. Int., 242, 3, doi:10.1093/gji/ggaf262.

Cetin, H. (1999). Water content changes along shear planes in drained and undrained triaxial compression tests on unsaturated cohesive soils, Turk. J. Eng. Environ. Sci., 23, 6, 465-471, 2587-1366.

Choy, G. L. and J. L. Boatwright (1995). Global patterns of radiated seismic energy and apparent stress, J. Geophys. Res. Solid Earth, 100, B9, 18205-18228, doi:10.1029/95JB01969.

Claesson, L., A. Skelton, C. Graham, C. Dietl et al. (2004). Hydrogeochemical changes before and after a major earthquake, Geology, 32, 8, 641-644, doi:10.1130/G20542.1.

Dobrovolsky, I. P., S. I. Zubkov and V. I. Miachkin (1979). Estimation of the size of earthquake preparation zones, Pure Appl. Geophys., 117, 5, 1025-1044, doi:10.1007/BF00876083.

Doglioni, C., S. Barba, E. Carminati and F. Riguzzi (2014). Fault on-off versus coseismic fluids reaction, Geosci. Front., 5, 6, 767-780, doi:10.1016/j.gsf.2013.08.004.

Druitt, T. H., R. A. Mellors, D. M. Pyle and R. S. J. Sparks (1989). Explosive volcanism on Santorini, Greece, Geol. Mag., 126, 2, 95-126, doi:10.1017/S0016756800006270.

Emre, Ö., T. Y. Duman, S. Özalp, S. Olgun et al. (2012). 1: 250000 ölçekli Türkiye Diri Fay Haritası. Maden Tetkik ve Arama Genel Müdürlüğü, Ankara – Türkiye.

Federico, C., L. Pizzino, D. Cinti, S. De Gregorio et al. (2008). Inverse and forward modelling of groundwater circulation in a seismically active area (Monferrato, Piedmont, NW Italy): Insights into stress-induced variations in water chemistry, Chem. Geol., 248, 1-2, 14-39, doi:10.1016/j.chemgeo.2007.10.007.

Friedrich, W. L. (2000) Fire in the Sea, Cambridge University Press, Cambridge, UK, 258.

Fytikas, M. (1990). Post-Minoan volcanic activity of the Santorini volcano, Volcanic hazard and risk, Forecasting possibilities, Thera and the Aegean world, III, 2, 183-198.

Galanopoulos, D., V. Sakkas, D. Kosmatos and E. Lagios (2005). Geoelectric investigation of the Hellenic subduction zone using long period magnetotelluric data, Tectonophysics, 409, 1-4, 73-84, doi:10.1016/j.tecto.2005.08.010.

Ganas, A., I. A. Oikonomou and C. Tsimi (2013). NOAfaults: a digital database for active faults in Greece, Bull. Geol. Soc. Greece, 47, 2, 518-530, doi:10.12681/bgsg.11079.

Gori, F. and M. D. Barberio (2022). Hydrogeochemical changes before and during the 2019 Benevento seismic swarm in central-southern Italy, J. Hydrol., 604, 127250, doi:10.1016/j.jhydrol.2021.127250.

Hanks, T. C. and H. Kanamori (1979). A moment magnitude scale, J. Geophys. Res. Solid Earth, 84, B5, 2348-2350, doi:10.1029/JB084iB05p02348.

Hickman, S., R. Sibson and R. Bruhn (1995). Introduction to special section: Mechanical involvement of fluids in faulting, J. Geophys. Res. Solid Earth, 100, B7, 12831-12840, doi:10.1029/95JB01121.

Hufstetler, R. S., E. E. Hooft, D. R. Toomey, B. P. VanderBeek et al. (2025). Seismic structure of the mid to upper crust at the Santorini-Kolumbo Magma System from joint earthquake and active source Vp-Vs tomography, Geochem. Geophys. Geosyst., 26, 4, doi:10.1029/2024GC012022.

İnan, S., T. Akgül, C. Seyis, R. Saatçılar et al. (2008). Geochemical monitoring in the Marmara region (NW Turkey): A search for precursors of seismic activity, J. Geophys. Res. Solid Eart, 113, B3, doi:10.1029/2007JB005206.

İnan, S., W. P. Balderer, F. Leuenberger-West, H. Yakan et al. (2012a). Springwater chemical anomalies prior to the Mw = 7.2 Van Earthquake (Turkey), Geochem. J., 46, e11-e16, doi:10.2343/geochemj.1.0159.

İnan, S., H. Çetin and N. Yakupoğlu (2024). Spring water anomalies before two consecutive earthquakes (M w 7.7 and M w 7.6) in Kahramanmaraş (Türkiye) on 6 February 2023, Nat. Hazards Earth Syst. Sci., 2, 2, 397-409, doi:10.5194/nhess-24-397-2024.

İnan, S., K. Ertekin, C. Seyis, S. Şimşek et al. (2010). Multi-disciplinary earthquake researches in Western Turkey: Hints to select sites to study geochemical transients associated to seismicity, Acta Geophys., 58, 767-813, doi:10.2478/s11600-010-0016-7.

İnan, S., A. Kop, H. Çetin, F. Kulak et al. (2012c). Seasonal variations in soil radon emanation: long-term continuous monitoring in light of seismicity, Nat. Hazards, 62, 575-591, doi:10.1007/s11069-012-0096-6.

İnan, S., Z. Pabuçcu, F. Kulak, S. Ergintav et al. (2012b). Microplate boundaries as obstacles to pre-earthquake strain transfer in Western Turkey: inferences from continuous geochemical monitoring, J. Asian Earth Sci., 48, 56-71, doi:10.1016/j.jseaes.2011.12.016.

Ingebritsen, S. E. and M. Manga (2014). Hydrogeochemical precursors, Nat. Geosci., 7, 10, 697-698, doi:10.1038/ngeo2261.

Isken, M. P., J. Karstens, P. Nomikou, M. M. Parks et al. (2025). Volcanic crisis reveals coupled magma system at Santorini and Kolumbo, Nature, 645, 8082, 939-945, doi:10.1038/s41586-025-09525-7.

Jackson, J. (1994). Active tectonics of the Aegean region, Annu. Rev. Earth Planet. Sci., 22, 239-271, doi:10.1146/annurev.ea.22.050194.001323.

Jolivet, L., C. Faccenna, B. Huet, L. Labrousse et al. (2013). Aegean tectonics: Strain localisation, slab tearing and trench retreat, Tectonophysics, 597, 1-33, doi:10.1016/j.tecto.2012.06.011.

Kanamori, H. (1977). The energy release in great earthquakes, J. Geophys. Res., 82, 20, 2981-2987, doi:10.1029/JB082i020p02981.

Lomax, A., V. Anagnostou, V. Karakostas, S. P. Hicks et al. (2025). The 2025 Santorini unrest unveiled: Rebounding magmatic dike intrusion with triggered seismicity, Science, 390, 6775, doi:10.1126/science.adz8538.

Luque-Espinar, J. A. and R. M. Mateos (2023). Hydrochemical changes in thermal waters related to seismic activity: The case of the 2020-2021 seismic sequence in Granada (S Spain), J. Hydrol., 627, 130390, doi:10.1016/j.jhydrol.2023.130390.

Malakootian, M. and J. Nouri (2010). Chemical variations of ground water affected by the earthquake in bam region Malakootian, Int. J. Environ. Res., 4, 3, 443-454, doi:10.22059/ijer.2010.229.

Martinelli, G. and A. Dadomo (2017). Factors constraining the geographic distribution of earthquake geochemical and fluid-related precursors, Chem. Geol., 469, 176-184, doi:10.1016/j.chemgeo.2017.01.006.

Martinelli, G., Y. Fu, Y. Li and F. Vallianatos (2023). Pre-earthquake observations and methods for earthquake forecasting and seismic hazard reduction, Front. Earth Sci., 11, 1150414, doi:10.3389/feart.2023.1150414.

Martinelli, G. and G. Tamburello (2020). Geological and geophysical factors constraining the occurrence of earthquake precursors in geofluids: a review and reinterpretation, Front. Earth Sci., 8, 596050, doi:10.3389/feart.2020.596050.

Mavroulis, S., M. Mavrouli, A. Sarantopoulou, A. Antonarakou et al. (2025). Increased Preparedness During the 2025 Santorini-Amorgos (Greece) Earthquake Swarm and Comparative Insights from Recent Cases for Civil Protection and Disaster Risk Reduction, GeoHazards, 6, 2, 32, doi:10.3390/geohazards6020032.

Newman, A. V., S. Stiros, L. Feng, P. Psimoulis et al. (2012). Recent geodetic unrest at Santorini caldera, Greece, Geophys. Res. Lett., 39, 6, doi:10.1029/2012GL051286.

Nicholson, K. (1993). Geothermal Fluids: Chemistry and Exploration Techniques, Springer Science and Business Media.

Nur, A. (1974). Matsushiro, Japan, earthquake swarm: confirmation of the dilatancy-fluid diffusion model, Geology, 2, 5, 217-221, doi:10.1130/0091-7613(1974)2<217:MJESCO>2.0.CO;2.

Nyst, M. and W. Thatcher (2004). New constraints on the active tectonic deformation of the Aegean, J. Geophys. Res. Solid Earth, 109, B11, doi:10.1029/2003JB002830.

Papastefanou, C., M. Manolopoulou, E. Savvides and S. Charalambous (1989). Radon monitoring at the Stivos Fault following the ML = 6.5 earthquake which occurred at Thessaloniki, Greece on 20 June 1978, Nucl. Geophys., 3, 49-56.

Papazachos, B. C. and D. G. Panagiotopoulos (1993). Normal faults associated with volcanic activity arc, Tectonophysics, 220, 1-4, 301-308, doi:10.1016/0040-1951(93)90237-E.

Papazachos, C., M. Foumelis, S. Bitharis, C. Pikridas et al. (2025). The Santorini 2024-2025 volcano-tectonic sequence: Constraining the initial phase of the intra-caldera unrest, Geophys. Res. Lett., 52, 13, doi:10.1029/2025GL115856.

Perez, N. M., P. A. Hernández, G. Igarashi, I. Trujillo et al. (2008). Searching and detecting earthquake geochemical precursors in CO2-rich groundwaters from Galicia, Spain, Geochem. J., 42, 1, 75-83, doi:10.2343/geochemj.42.75.

Perissoratis, C. (1995). The Santorini volcanic complex and its relation to the stratigraphy and structure of the Aegean arc, Greece, Mar. Geol., 128, 1-2, 37-58, doi:10.1016/0025-3227(95)00090-L.

Pulinets, S. A., V. A. Alekseev, A. D. Legen'ka and V. V. Khegai (1997). Radon and metallic aerosols emanation before strong earthquakes and their role in atmosphere and ionosphere modification, Adv. Space Res., 20, 11, 2173-2176, doi:10.1016/S0273-1177(97)00666-2.

Reilinger, R., S. McClusky, P. Vernant, S. Lawrence et al. (2006). GPS constraints on continental deformation in the Africa-Arabia-Eurasia continental collision zone and implications for the dynamics of plate interactions, J. Geophys. Res. Solid Earth, 111, B5, doi:10.1029/2005JB004051.

Rikitajke, T. (1979). Classification of earthquake precursors, Tectonophysics, 54, 3-4, 293-309, doi:10.1016/0040-1951(79)90372-X.

Rikitake, T. (1987). Earthquake precursors in Japan: precursor time and detectability, Tectonophysics, 136, 3-4, 265-282, doi:10.1016/0040-1951(87)90029-1.

Rojstaczer, S., S. Wolf and R. Michel (1995). Permeability enhancement in the shallow crust as a cause of earthquake-induced hydrological changes, Nature, 373, 6511, 237-239, doi:10.1038/373237a0.

Scholz, C. H., L. R. Sykes and Y. P. Aggarwal (1973). Earthquake Prediction: A Physical Basis: Rock dilatancy and water diffusion may explain a large class of phenomena precursory to earthquakes, Science, 181, 4102, 803-810, doi:10.1126/science.181.4102.803.

Sibson, R. H. (1992). Implications of fault-valve behaviour for rupture nucleation and recurrence, Tectonophysics, 211, 1-4, 283-293, doi:10.1016/0040-1951(92)90065-E.

Skelton, A., M. Andrén, H. Kristmannsdóttir, G. Stockmann et al. (2014). Changes in groundwater chemistry before two consecutive earthquakes in Iceland, Nat. Geosci., 7, 10, 752-756, doi:10.1029/2018JB016757.

Skelton, A., L. Claesson, G. Chakrapani, C. Mahanta et al. (2008). Coupling between seismic activity and hydrogeochemistry at the Shillong Plateau, Northeastern India, Pure Appl. Geophys., 165, 45-61, doi:10.1007/s00024-007-0288-2.

Skelton, A., L. Liljedahl-Claesson, N. Wästeby, M. Andrén et al. (2019). Hydrochemical changes before and after earthquakes based on long-term measurements of multiple parameters at two sites in northern Iceland – A Review, J. Geophys. Res. Solid Earth, 124, 2702-2720, doi:10.1029/2018JB016757.

Sugisaki, R., T. Ito, K. Nagamine and I. Kawabe (1996). Gas geochemical changes at mineral springs associated with the 1995 southern Hyogo earthquake (M = 7.2), Japan, Earth Planet. Sci. Lett., 139, 1-2, 239-249, doi:10.1016/0012-821X(96)00007-6.

Sultankhodhaev, G. A. (1984). International Symposium on Earthquake Prediction, UNESCO, Paris, 181-191, last access 14 April 2025, https://unesdoc.unesco.org/ark:/48223/pf0000063090.

Taymaz, T., J. Jackson and D. McKenzie (1991). Active tectonics of the north and central Aegean Sea, Geophys. J. Int., 106, 2, 433-490, doi:10.1111/j.1365-246X.1991.tb03906.x.

Thomas, D. M., K. E. Cuff and M. E. Cox (1986). The association between ground gas radon variations and geologic activity in Hawaii, J. Geophys. Res. Solid Earth, 91, 12186-12198, doi:10.1029/JB091iB12p12186.

Toker, M., E. Yavuz and E. Balkan (2025). Focal mechanisms and bouguer-gravity anomalies of the 2025 earthquake cluster in the Santorini-Amorgos region (Southern Aegean Sea, Greece): evidence for shallow extensional magmatism, J. Seismol., 29, 4, 943-961, doi:10.1007/s10950-025-10314-y.

Toutain, J. P., M. Munoz, F. Poitrasson and A. C. Lienard (1997). Springwater chloride ion anomaly prior to a ML = 5.2 Pyrenean earthquake, Earth Planet. Sc. Lett., 149, 1-4, 113-119, doi:10.1016/S0012-821X(97)00066-6.

Triantafyllou, I., G. A. Papadopoulos, C. Siettos and K. Spiliotis (2025). Real-Time Foreshock-Aftershock-Swarm Discrimination During the 2025 Seismic Crisis near Santorini Volcano, Greece: Earthquake Statistics and Complex Networks, Geosci. J., 15, 8, 300, doi:10.3390/geosciences15080300.

Tsunogai, U. and H. Wakita (1995). Precursory chemical changes in ground water: Kobe earthquake, Japan, Science, 269, 5220, 61-63, doi:10.1126/science.269.5220.61.

Wakita, H. (1996). Geochemical challenge to earthquake prediction, Proc. Natl. Acad. Sci. USA., 93, 9, 3781-3786, doi:10.1073/pnas.93.9.3781.

Wang, Y., X. Zhou, J. Li, Y. Bai et al. (2025). Hydrogeochemical characteristics of hot springs in the Longriba fault, northeastern Tibetan Plateau: Tectonic implications for geothermal fluid circulation, J. Asian Earth Sci., 281, 106511, doi:10.1016/j.jseaes.2025.106511.

Xiang, Y. and S. Peng (2023). Hydrochemical and stable isotopes (δ2H and δ18O) changes of groundwater from a spring induced by local earthquakes, Northwest China, Front. Earth Sci., 10, 1100068, doi:10.3389/feart.2022.1100068.

Yakupoğlu, N., A. Sabuncu, C. Erbil, E. Kırkan et al. (2025). Pre-earthquake hydrogeochemical anomalies in spring waters: two distinctive cases from western Türkiye, J. Hydrol., 133920, doi:10.1016/j.jhydrol.2025.133920.

Yan, Y., Z. Zhang, X. Zhou, G. Wang et al. (2024). Geochemical characteristics of hot springs in active fault zones within the northern Sichuan-Yunnan block: Geochemical evidence for tectonic activity, J. Hydrol., 635, 131179, doi:10.1016/j.jhydrol.2024.131179.

Zeng, Z., X. Zhou, J. Dong, J. Li et al. (2025). Seismic Signals of the Wushi MS 7.1 Earthquake of 23 January 2024, Viewed Through the Angle of Hydrogeochemical Characteristics, Appl. Sci., 5, 9, 4791, doi:10.3390/app15094791.

Zeyrek, M., K. Ertekin, S. Kacmaz, C. Seyis et al. (2010). An ion chromatography method for the determination of major anions in geothermal water samples, Geostand. Geoanal. Res., 34, 1, 67-77, doi:10.1111/j.1751-908X.2009.00020.x.

***CORRESPONDING AUTHOR: Nurettin YAKUPOĞLU**,
İstanbul Technical University, Faculty of Mines, Department of Geological Engineering, Ayazağa, 34469, İstanbul, Türkiye
e-mail: yakupoglu@itu.edu.tr